C(sp 2)–Coupled Nitronyl Nitroxide and Iminonitroxide Diradicals

ARTICLE *in* CHEMISTRY - A EUROPEAN JOURNAL · MARCH 2014

Impact Factor: 5.73 · DOI: 10.1002/chem.201302681 · Source: PubMed

ChemPubSoc Europe

DOI: 10.1002/chem.201302681

CHEMISTRY A European Journal Full Paper

Singlet Diradicals

C(sp^2)-Coupled Nitronyl Nitroxide and Iminonitroxide Diradicals

Svyatoslav Tolstikov,[a] Evgeny Tretyakov,[a] Sergey Fokin,[a] Elizaveta Suturina,[b] Galina Romanenko,[a] Artem Bogomyakov,[a] Dmitri Stass,[b] Alexander Maryasov,[b] Matvey Fedin,[a] Nina Gritsan,*[b] and Victor Ovcharenko*[a]

Abstract: Spin-labelled compounds are widely used in chemistry, physics, biology and the materials sciences but the synthesis of stable high-spin organic molecules is still a challenge. We succeeded in synthesising heteroatom analogues of the 1,1,2,3,3-pentamethylenepropane (PMP) diradicals with two nitronyl nitroxide (**DR^1**) and with two iminonitroxide (**DR^2**) fragments linked through the C(sp^2) atom of the nitrone group. According to magnetic susceptibility measurements, EPR data and ab initio calculations at the (8,6)CASSCF and (8,6)NEVPT2 levels, **DR^1** and **DR^2** have singlet ground states. The singlet–triplet energy splitting (2*J*) is low ($J/k = -7.4$ for **DR^1** and -6.0 K for **DR^2**), which comes from the disjoint nature of these diradicals. The reaction of [Cu(hfac)$_2$] with **DR^1** gives rise to different heterospin complexes in which the diradical acts as a rigid ligand, retaining its initial conformation. For the [{Cu(hfac)$_2$}$_2$(**DR^1**)(H$_2$O)] complex, sufficiently strong ferromagnetic interactions ($J_1/k = 42.7$ and $J_2/k = 14.1$ K) between two coordinating Cu^{II} ions and **DR^1** were revealed. In [{Cu(hfac)$_2$}$_2$(**DR^1**)(H$_2$O)][Cu(hfac)$_2$(H$_2$O)], the very strong and antiferromagnetic ($J/k = -416.1$ K) exchange interaction between one of the coordinating Cu^{II} ions and **DR^1** is caused by the very short equatorial Cu–O bond length (1.962 Å).

Introduction

The synthesis of high-spin organic molecules is a challenge in the field of molecular-based magnets,[1] for which exchange interactions between the spin centres play a crucial role in determining the bulk magnetic properties.[2] The nature of the exchange interactions is particularly important when the diradicals (or polyradicals) serve as a bridging function linking paramagnetic metal ions to form complex heterospin structures.[3] The magnitude and sign of the intramolecular exchange interactions in high-spin organic molecules are difficult to predict[4] and their determination requires thorough investigation.[5]

Notably, among a family of organic diradicals, there are only a few examples of C(sp^3)-spaced diradicals,[2b,6] whereas C(sp^2)-spaced nitronyl nitroxide or iminonitroxide diradicals of general type **DR** are unknown.[7] Herein, we report the synthesis of C(sp^2)-spaced nitronyl nitroxide (**DR^1**) and iminonitroxide (**DR^2**) diradicals. These diradicals have been isolated and characterized by single-crystal X-ray diffraction, EPR spectroscopy and magnetic susceptibility measurements. Some experimental results are supported by quantum chemical calculations. Furthermore, heterospin complexes of [Cu(hfac)$_2$] (hfac = hexafluoroacetylacetonato) with **DR^1** were synthesised. This demonstrates the ability of this type of diradicals to act as bridging ligands in complex heterospin systems.

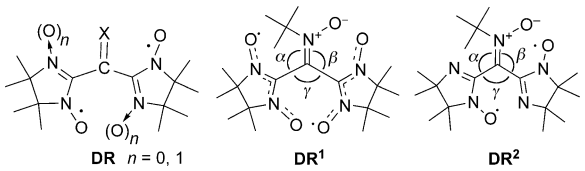

Results and Discussion

Synthesis, structure and magnetic properties of the diradicals

An efficient method for preparing paramagnetic lithium derivative **3** (Scheme 1) was recently developed,[8] which paved the way towards the synthesis of previously unavailable nitroxides.[9] Takui et al. obtained the highly compact nitroxide trimethylenemethane analogue by reacting **3** with 2-methyl-2-nitrosopropane, followed by oxidation of the product.[10] These developments prompted us to use **3** in preparing the first C(sp^2)-spaced nitronyl nitroxide diradical **DR^1**.

We found that **DR^1** could be obtained in yields of about 20% after reacting compound **3** with silicon derivative **4**. The ensuing deoxygenation of **DR^1** by use of the AcOH/NaNO$_2$

[a] Dr. S. Tolstikov, Prof. E. Tretyakov, Dr. S. Fokin, Prof. G. Romanenko, Dr. A. Bogomyakov, Prof. M. Fedin, Prof. V. Ovcharenko
International Tomography Center, SB RAS
Institutskaya Str., 3A, 630090 Novosibirsk (Russia)
E-mail: victor.ovcharenko@tomo.nsc.ru

[b] Dr. E. Suturina, Dr. D. Stass, Dr. A. Maryasov, Prof. N. Gritsan
Institute of Chemical Kinetics and Combustion, SB RAS
Institutskaya Str., 3, 630090 Novosibirsk (Russia)
E-mail: gritsan@kinetics.nsc.ru

Supporting information for this article is available on the WWW under http://dx.doi.org/10.1002/chem.201302681. The supporting information includes the data of X-ray structure analysis for **6** and **7**, SQUID and EPR data for **DR^1** and **DR^2**, and results of quantum chemical calculations.

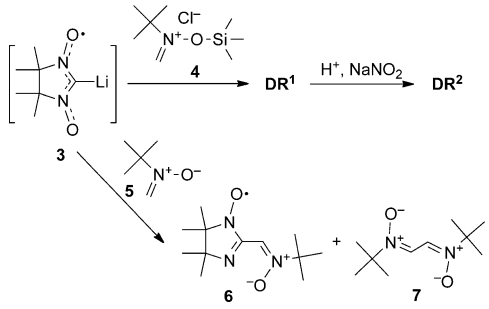

Scheme 1. Reactions of spin-labelled **3** with nitrone **5** and its silicon derivative **4**.

system produced **DR²** with yields of up to 80%. It is worth noting that interaction of **3** with nitrone **5** resulted in a complex mixture of products, from which only (*Z*)-*N*-*tert*-butyl-1-(1-oxyl-4,4,5,5-tetramethyl-4,5-dihydro-1*H*-imidazol-2-yl)methanimine oxide (**6**, yield 5–10%) and *N*,*N*′-(ethane-1,2-diylidene)-bis(2-methylpropan-2-amine *N*-oxide) (**7**, yield < 1%) could be isolated (Scheme 1).

Single crystals for XRD experiments were obtained by allowing solutions of **DR¹**, **DR²**, **6** or **7** in a mixture of CH_2Cl_2 and *n*-heptane at 5 °C to slowly evaporate. Figure 1 shows the molecular structures of the diradicals (data for **6** and **7** are given in the Supporting Information). In the structure of **DR¹**, the O(8)–N(8), O(28)–N(27), O(17)–N(16) and O(19)–N(19) bond lengths are typical for nitronyl nitroxides (Table 1). In turn, the bond lengths of the NCNO fragments of **DR²** are also typical of the iminonitroxide family. At the same time, both diradicals **DR¹**

Table 1. Bond lengths [Å] and dihedral and torsion angles [°] in free **DR¹** and **DR²** and in the complexes of [Cu(hfac)$_2$] with **DR¹**.

	DR¹	DR²	10[b]		11[b]
T [K]	295	240	85	240	295
O(5)–N(4)	1.271(2)	1.274(2)	1.266(5)	1.262(3)	1.278(5)
			1.277(5)	1.265(3)	
O(8)–N(8)	1.274(2)		1.285(5)	1.280(3)	1.281(4)
			1.295(4)	1.287(3)	
O(17)–N(16)	1.281(2)	1.275(2)	1.277(4)	1.290(3)	1.271(5)
			1.282(4)	1.278(3)	
O(19)–N(19)	1.281(2)		1.289(5)	1.276(4)	1.264(6)
			1.276(4)	1.275(3)	
O(28)–N(27)	1.273(2)	1.268(2)	1.301(5)	1.292(3)	1.287(5)
			1.299(5)	1.299(3)	
∡N(4)C(6)–C(7)N(8)	57.2(3)	57.3(3)	−62.4(7)	−60.3(5)	−68.0(9)
			−57.0(7)	−57.3(5)	
∡N(4)C(6)–C(18)N(19)	−141.4(2)	−139.6(2)	133.4(4)	131.3(3)	138.9(6)
			130.5(4)	131.7(3)	
∡Ia–III[a]	73.59(8)		68.0(1)	67.5(1)	66.0(2)
			66.5(1)	67.0(1)	
∡Ib–III[a]	54.5(1)		55.9(4)	56.1(2)	53.5(2)
			55.5(3)	57.0(2)	
∡IIa–III[a]		74.9(1)			
∡IIb–III[a]		53.1(2)			

[a] Fragment O(8)N(8)C(7)N(16)O(17) is denoted as Ia, O(19)N(19)C(18)N(27)O(28) as Ib, N(8)C(7)N(16)O(17) as IIa, N(19)C(18)N(27)O(28) as IIb and O(5)N(4)C(6)C(1) as III. [b] Complex **10**: [{Cu(hfac)$_2$}$_2$(**DR¹**)(H$_2$O)]; complex **11**: [{Cu(hfac)$_2$}$_2$(**DR¹**)(H$_2$O)][Cu(hfac)$_2$-(H$_2$O)].

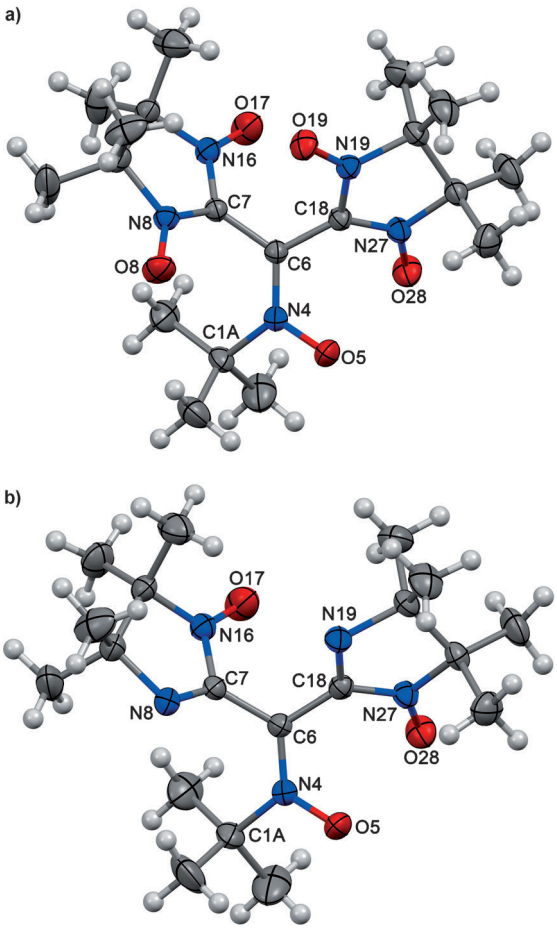

Figure 1. View of a) **DR¹** and b) **DR²** molecules. Thermal ellipsoids are shown with 35% probability.

and **DR²** demonstrate unprecedented shortening of the N(4)–O(5) bond in the nitrone fragment compared with the typical N^+–O^- bond lengths in acyclic nitrones (1.29–1.30 Å).[7] Indeed, before this investigation the shortest N^+–O^- bond lengths, 1.284–1.289 Å, were observed in two acyclic *tert*-butylnitrones (**BN**s).[11]

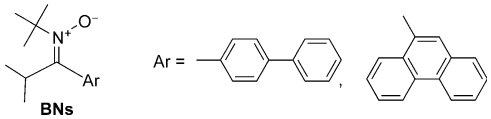

The sum of the bond angles around the C6 atom (denoted α, β and γ in the structures of **DR¹** and **DR²**) is equal to 359.6° for **DR¹** and 358.6° for **DR²**, indicating that the nitrone part of the molecule has an almost planar structure. The dihedral angles between the mean planes of the nitronyl nitroxide (Ia, IIa) and nitrone (III) fragments, ∡Ia–III and ∡IIa–III, and the angles ∡Ib–III and ∡IIb–III (Ib, IIb–iminonitroxide fragments) are very similar (Table 1). The paramagnetic fragments Ia,b (or IIa,b) are significantly twisted relative to both each other and to the nitrone fragment III. This gives rise to rather short intramolecular distances between atoms O(19) and C(7) in **DR¹** and atoms O(17) and C(18) in **DR²** of only 2.844(2) and 3.164(3) Å, respectively. These distances, as well as the intramolecular dis-

tances between atoms O(5) and O(28) (2.723(2) in **DR[1]** and 2.758(2) Å in **DR[2]**), are much shorter than the intermolecular distances between the nitroxide oxygen atoms of fragments Ia and Ib or IIa and IIb, which exceed 4.5 Å.

The diradical natures of **DR[1]** and **DR[2]** were confirmed by registration of their EPR spectra. Figure 2 shows the EPR spectrum

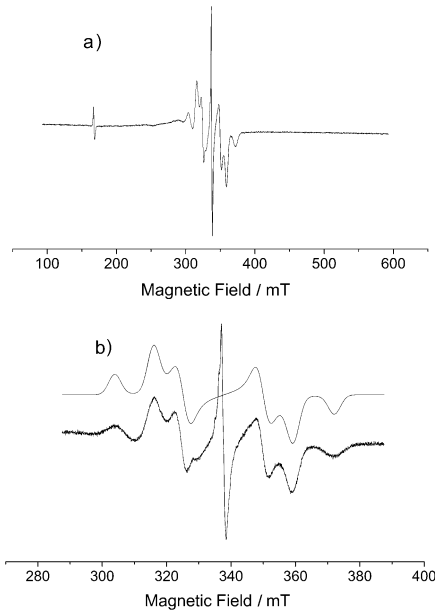

Figure 2. EPR spectra of **DR[2]** in glassy *ortho*-terphenyl taken at a microwave power of 2 mW and modulation amplitude of 0.2 mT for the a) full-range spectrum and b) an expanded view of the region around $g=2$ (noisy lower trace) and the model spectrum (upper trace) by using the spin Hamiltonian in Equation (1).

of **DR[2]** in glassy *ortho*-terphenyl at 200 K, which is characteristic of a triplet diradical.[12] The spectrum consists of a Pake doublet around 340 mT ($g\approx2$), arising from dipolar coupling between two electron spins, and an additional weaker signal in the half-field region ($g\approx4$). Figure 2b gives an expanded view of the EPR spectrum around $g\approx2$ and a spectrum simulation by using second-order perturbation theory and Gaussian shapes for the individual lines. The spectrum was simulated by using the following spin Hamiltonian [$S=1$; Eq. (1)], in which ω_0 is the Zeeman frequency for electron spin; z is the direction of the external magnetic field; X, Y and Z are the principal axes of the zero-field splitting (ZFS) tensor; and D and E are the principal values of this tensor.

$$\hat{H}=\hbar\omega_0\hat{S}_z+D\left[\hat{S}_Z^2-{}^2\!/_3\right]+E\left[\hat{S}_X^2-\hat{S}_Y^2\right] \quad (1)$$

Positions of the resonance lines around $g=2$ ($B_\perp$) were calculated by using Equation (2), in which h is the Plank constant, ν is the working frequency of the EPR spectrometer, μ_B is the Bohr magneton, g is the g factor of the diradical, $d_k=\mathbf{n}^T\mathbf{D}^k\mathbf{n}$, **n** is a unit vector along the external magnetic field, **D** is the zero-field splitting tensor, superscript T means a matrix transposition, and Tr(**X**) and det(**X**) are the trace and determinant of matrix **X**, respectively.[13] The simulated spectrum is a sum of the doublets given by Equation (2) over all possible orientations of the vector **n**; the number of orientations was chosen to obtain a smooth spectrum. The "sticky" spectrum was then convoluted with the derivative of the Gaussian function with the proper dispersion. As in our experimental conditions, the Zeeman interaction is much stronger than zero-field splitting, and the thermal energy is much greater than the Zeeman one; only the absolute D values [Eq. (1)] could be obtained from the experiments.[13]

$$h\nu=g\mu_B B_\perp\pm\frac{3}{2}d_1+\frac{1}{4g\mu_B B_\perp}\left\{d_2-\frac{3}{2}d_1^2+\frac{1}{2}[Tr(\mathbf{D}^2)-2d_{-1}\det(\mathbf{D})]\right\} \quad (2)$$

The best fitting was obtained with the following ZFS parameters: $D=34.1$ mT, $E=3.1$ mT ($E/D=0.091$), and the width of the Gaussian-shaped lines = 1.9 mT, which coincides with the width of the spectrum in the half-field region. The effective distance between the radical centres estimated in the point–dipole approximation (r) is 0.43 nm.

The ZFS parameters for the XRD structure of **DR[2]** have been calculated at the ROBP88/TZVP level[14] and found to be $D=-27.9$ mT and $E/D=0.043$, in reasonable agreement with experiments, although the E value is noticeably underestimated. A good agreement with experiment indicates that our calculations give the correct spin-density distribution in the triplet state of diradical **DR[2]**. The line width of 1.9 mT is consistent with the hyperfine couplings predicted at the UB3LYP/TZVP level;[14c,15] the computed isotropic and anisotropic (A_{zz}) hyperfine coupling constants for four N atoms in **DR[2]** are in the range 0.20–0.24 and 0.95–1.33 mT, respectively.

There is also an additional narrow signal at $g\approx2$, which was not considered in the simulation (Figure 2b). This signal was present only at low microwave power and rapidly saturated at higher powers, indicating that the narrow signal belongs to an unidentified radical species. Double integration demonstrates that despite its prominence in the derivative spectrum, the narrow signal accounts for only about 0.3% of the total signal intensity.

The EPR spectrum of diradical **DR[1]** (Figure 3) is similar to the spectrum of **DR[2]**. Because of the poor solubility of **DR[1]** in *ortho*-terphenyl, the spectra were recorded at low concentration to avoid precipitation of the diradical as precipitation leads to glass cracking and poor quality spectra. The lower concentration of **DR[1]** explains the slightly worse *S/N* ratio of the full-range spectrum (Figure 3a).

The spectrum in the vicinity of $g\approx2$ was taken at a higher microwave power to reduce the contribution of the narrow signal and to improve the *S/N* ratio for the diradical signal. Both effects are important to improve the quality of the model presented in Figure 3b. In contrast to diradical **DR[2]**, the EPR spectrum of **DR[1]** can be reproduced only as a superposition of the spectra of two diradicals having markedly different sets of ZFS parameters. The best fitting was obtained with the following two sets of parameters: $D_1=29.9$ mT, $E_1=5.1$ mT ($E_1/D_1=0.17$) and $D_2=23.6$ mT, $E_2=2.0$ mT ($E_2/D_2=0.085$). These D

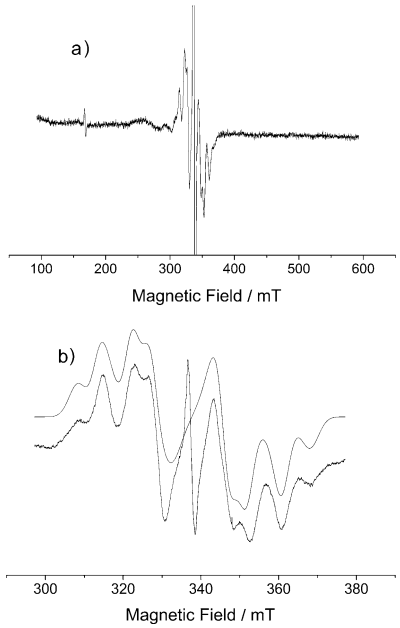

Figure 3. EPR spectra of **DR[1]** in glassy *ortho*-terphenyl at 200 K for the a) full-range spectrum recorded at a microwave power of 2 mW and b) an expanded view of the region around $g \approx 2$ (noisy lower trace recorded at a microwave power of 200 mW), and a model of the EPR spectrum by using the spin Hamiltonian in Equation (1) with two sets of ZFS parameters (upper trace). In both cases, the modulation amplitude was 0.2 mT.

values correspond to the following effective distances between the radical centres, estimated in the point–dipole approximation, $r_1 = 0.45$ and $r_2 = 0.49$ nm. The corresponding widths of the Gaussian-shaped lines are 2.2 and 1.7 mT, and the relative contributions of the two components are 1:0.7. It should be noted that both the D_1 and D_2 values are noticeably smaller than the D parameter for **DR[2]**. The first set of ZFS parameters also demonstrates an unexpectedly high E/D ratio, which is about half of its maximum possible value (1/3).

By using the same method as in the calculations for **DR[2]** (ROBP88/TZVP[14]), we calculated the ZFS parameters for diradical **DR[1]**. Calculations performed by using the XRD-structure predicted $D = -22.3$ mT and $E/D = 0.082$ values. In agreement with experiment, the D value is noticeably smaller and the E/D ratio is significantly larger than the corresponding values calculated for **DR[2]**. As samples for EPR measurements were prepared in molten *ortho*-terphenyl, the geometry of diradical **DR[1]** may differ from its XRD structure. Thus, we optimized the geometry of **DR[1]** at the UB3LYP/TZVP level,[14c,15] starting from the XRD structure. The geometry corresponding to the minimum on the potential energy surface (PES) differs only slightly from the XRD geometry (e.g., the dihedral angle ∢N(4)C(6)C(18)N(19) in the two geometries is equal to −135.3 and −141.4°, respectively) and leads to similar calculated ZFS parameters, $D = -21.9$ mT and $E/D = 0.065$.

As mentioned earlier, two types of diradical **DR[1]** with appreciably different ZFS parameters have been proposed to reproduce the experimental EPR spectrum. To explain this fact, we tried to find the second minimum on the PES of **DR[1]**. By rotating the *t*Bu-N^+-O^- substituent about the N(4)C(6) bond (see Figure 1 for numbering), we were able to find this second minimum, with a relative enthalpy of 1.5 kcal mol^{-1} and relative free energy of 1.2 kcal mol^{-1} (gas-phase computations at the UB3LYP/TZVP level). However, the ZFS parameters calculated for this structure ($D = -21.8$ mT and $E/D = 0.068$) are very similar to those calculated for both the first minimum and XRD structures. Thus, we cannot currently give a reasonable explanation for the two-component EPR spectrum of **DR[1]**.

The bulk magnetic properties of the diradicals were investigated by measuring the temperature dependence of the molar magnetic susceptibility (χ). For both diradicals, the effective magnetic moments ($\mu_{eff} \approx (8\chi T)^{1/2}$) are almost independent of the temperature in the range 50–300 K and reach the value of 2.42 μ_B at room temperature (Figure 4 and Figure S4 in the

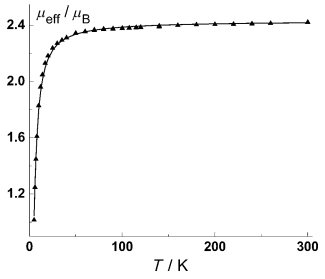

Figure 4. The temperature dependence of μ_{eff} for **DR[1]**. The solid line presents the best fitting based on the Bleaney–Bowers equation with $J/k = -7.4$ K.

Supporting Information). This value is close to 2.45 μ_B, which is typical of two weakly coupled paramagnetic centres with $S = 1/2$ and $g = 2$. Note that with a strong ferromagnetic coupling this value is equal to 2.83 μ_B. Cooling the samples to the temperature range 50–5 K leads to a significant decrease in μ_{eff} to 1.02 μ_B for **DR[1]** and 1.30 μ_B for **DR[2]**. The decrease in μ_{eff} indicates the dominance of the antiferromagnetic (AF) interactions between the paramagnetic centres for both compounds.

According to the UB3LYP calculations, the spin density is localised almost exclusively at the nitronyl nitroxide (**DR[1]**) or iminonitroxide (**DR[2]**) fragments (Figure 5). Only a small negative spin density is localised on the linker group, −0.07 for **DR[1]** and −0.06 for **DR[2]**. Thus, to estimate the exchange interactions between diradicals, we performed broken-symmetry calculations at the UB3LYP/SVP level[15,16] for pairs of **DR[1]** or **DR[2]** with the shortest distances between the paramagnetic fragments (Figure S5 in the Supporting Information).

According to these calculations, the J/k values were found to be negligible, namely, 0.2 and 0.3 K for the closest **DR[1]**···**DR[1]** and **DR[2]**···**DR[2]** pairs, respectively (Figure S5, Table S1 in the Supporting Information). Thus, the temperature dependences of the effective magnetic moments (Figure 4 and Figure S4 in the Supporting Information) were approximated by using the Bleaney–Bowers equation.[17] The best agreement with experiment was achieved with J/k values and g factors equal to −7.4 K and 2.0 for **DR[1]** and −6.0 K and 2.0 for **DR[2]**. Therefore, the new diradicals are ground-state singlets with a very small singlet–triplet splitting. We also proved this with EPR measure-

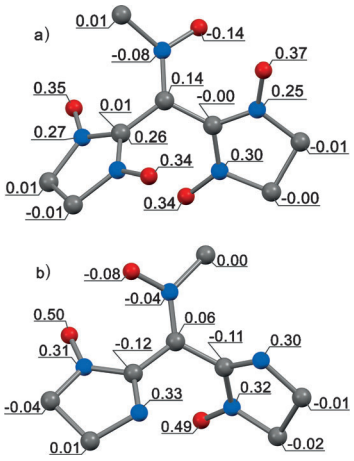

Figure 5. Mulliken atomic spin densities calculated at the UB3LYP/TZVP level for a) **DR[1]** and b) **DR[2]**. The methyl substituents are omitted for clarity.

ments on diradicals **DR[1]** and **DR[2]** in the solid state and in strongly diluted frozen solutions. The obtained EPR data confirm that the singlet–triplet splitting in these diradicals is about or smaller than 14 K and that for **DR[2]** the ground state is a singlet (Figures S2 and S3 in the Supporting Information).

Recently, stable nitroxide-substituted nitronyl nitroxide (**8**) and iminonitroxide (**9**) diradicals were synthesised and their magnetic properties were studied.[10,18] These diradicals are heteroatomic analogues of trimethylenemethane (TMM) and, similar to the parent TMM diradical,[19] they are triplet ground-state species with large enough J/k values, estimated experimentally to be 390 and approximately 550 K for **8** and **9**, respectively.[10,18] Our previous calculations at the UB3LYP/TZVP level predicted $J/k = 439$ K for **8**, in very good agreement with experiment ($\approx$400 K).[18]

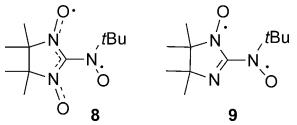

8 **9**

Thus, we calculated the J values for **DR[1]** and **DR[2]** at the same level of theory by using the XRD geometry of the diradicals. Unfortunately, in contrast to the experiments, the calculations predicted positive J/k values of 159 for **DR[1]** and 34.0 K for **DR[2]**. Therefore, we performed more rigorous multi-reference calculations. To properly take into account the static electronic correlation, we calculated the singlet–triplet splitting (ΔE_{ST}) at the (8,6)CASSCF/SVP level. The active space consisting of six molecular orbitals is presented in the Supporting Information (Figure S6). For both diradicals, the J/k values were calculated to be negative and very small (-1.4 and -0.6 K for **DR[1]** and **DR[2]**, respectively). Accounting for dynamic electron correlation at the (8,6)NEVPT2/SVP level of theory led to J/k values equal to -6.8 and -3.4 K for **DR[1]** and **DR[2]**, respectively, in perfect agreement with the experiments (-7.4 and -6.0 K).

However, so perfect an agreement between theory and experiment is rather accidental. For example, in the case of **DR[2]** an increase in the active space to eight MOs led to very small but positive J/k values (1.5 at the CASSCF level and 3.8 K at the NEVPT2 level). Thus, we can only conclude that, in agreement with experiment, the multi-reference calculations predict almost degenerate singlet and triplet states of diradicals **DR[1]** and **DR[2]**.

In contrast to **8** and **9**, being the heteroatom analogues of TMM and having triplet ground states, diradicals **DR[1]** and **DR[2]** are heteroatom analogues of 1,1,2,3,3-pentamethylenepropane (PMP, Figure 6). In their seminal work,[20] Borden and Davidson

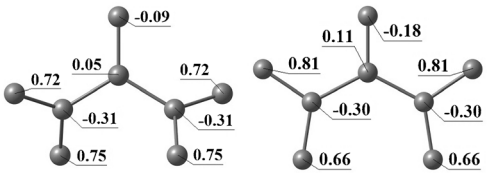

Figure 6. Mulliken atomic spin densities calculated at the UB3LYP/TZVP level for the triplet state of the parent hydrocarbon diradical PMP with a fully optimized geometry (left, approximately C_2 symmetry) and with a partially optimized geometry of C_{2v} symmetry (right). Hydrogen atoms are omitted for clarity.

pointed out that PMP is an example of a diradical with disjoint (confined to different regions of space) nonbonding MOs (NBMOs). In the case of PMP, the NBMOs were proposed to be those of the two isolated allyl radicals, and almost degenerate singlet and triplet states of PMP were predicted.[20] Thus, **DR[1]** and **DR[2]**, being stable analogues of PMP, can also be expected to have almost degenerate triplet and singlet states.

To better understand the properties of our diradicals, we analysed in detail the electronic structure of the parent PMP diradical—the simplest model of **DR[1]** and **DR[2]**. To the best of our knowledge, the value of ΔE_{ST} for PMP has been calculated at a high enough level of theory (up to SDTQ-CI) for a partially optimized structure of the C_{2v} symmetry.[21] PMP was predicted to have a triplet ground state with a very small ΔE_{ST} ($\approx$1.5 kcal mol^{-1}, $J/k \approx 190$ K) compared to the ΔE_{ST} (16.1 ± 0.2 kcal mol^{-1})[19] of the non-disjoint TMM diradical.

We performed both the full and partial (keeping C_{2v} symmetry) geometry optimization of the triplet PMP diradical at the UB3LYP/TZVP level. We found that the minimum on the PES corresponds to the nonplanar structure of C_2 symmetry (Figure 6, left). In turn, the planar C_{2v} structure is characterized by two imaginary frequencies and its relative energy is 15 kcal mol^{-1}. Nevertheless, we calculated the singlet–triplet splitting for both structures by using the spin-unrestricted broken-symmetry approach, as well as multi-reference CASSCF and NEVPT2 methods (Table 2). The active space consisted of the eight π MOs (Figures S7 and S8 in the Supporting Information) and all eight π electrons were involved in the CASSCF calculations.

Table 2 demonstrates that, in agreement with previous calculations,[21] the planar PMP has a triplet ground state with a small J/k value (100–200 K). However, the minimum on the triplet PES corresponds to a nonplanar structure characterized

Table 2. Parameters of the exchange interactions (J/k) for 1,1,2,3,3-pentamethylenepropane diradical calculated at different levels of theory.

Method	J/k [K]	
	planar C_{2v}	non-planar C_2
BS-UB3LYP/TZVP	171	−262
(8,8)CASSCF/SVP	114	−94
(8.8)NEVPT2/SVP	78	−142

by a small AF interaction with $J/k = -142$ K at the highest level of theory employed. For both structures (C_{2v} and C_2), the sum and difference SOMOs are indeed the allyl-type orbitals with very little overlap (Figures S7 and S8 in the Supporting Information). Thus, the interaction between electrons on these new SOMOs is very small. Note that overlap of these orbitals, although negligible in both cases, is smaller in the nonplanar C_2 structure.

The hetero-substitution of the hydrocarbon diradicals leads to a significant decrease in the singlet–triplet splitting.[10,18,22] Thus, the nonplanar **DR^1** and **DR^2**, being the heteroatom analogues of PMP, have small and negative J values, and the main reason for this is the disjoint nature of their NBMOs.

Synthesis, structure, and magnetism of [Cu(hfac)$_2$] complexes with DR^1

We attempted to create more complex multi-spin systems on the basis of these new diradicals. Diradical **DR^2** and [Cu(hfac)$_2$] crystallised separately in the different solvents used. In contrast with **DR^2**, we succeeded with diradical **DR^1** in synthesizing and isolating in crystal form two heterospin complexes, that is, [{Cu(hfac)$_2$}$_2$(**DR^1**)(H$_2$O)] (**10**) and [{Cu(hfac)$_2$}$_2$(**DR^1**)(H$_2$O)][Cu(hfac)$_2$(H$_2$O)] (**11**; Scheme 2). XRD structures of these complexes

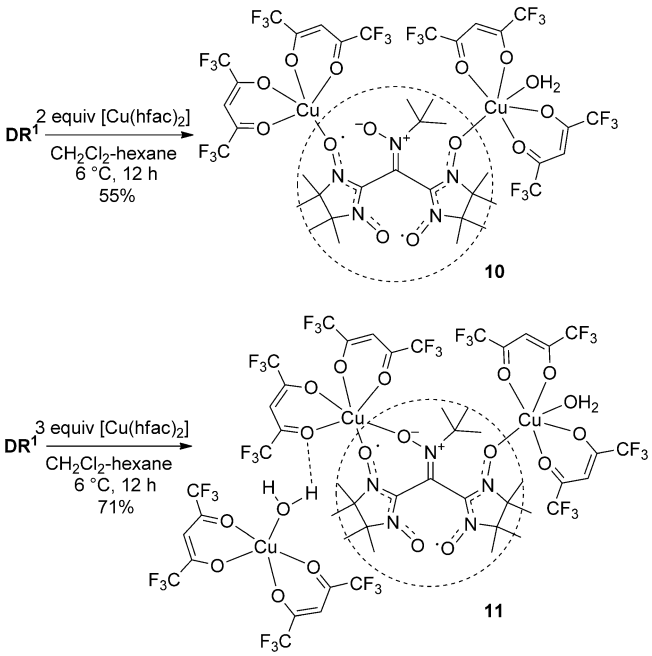

Scheme 2. Complexes obtained by reaction of [Cu(hfac)$_2$] with **DR^1**.

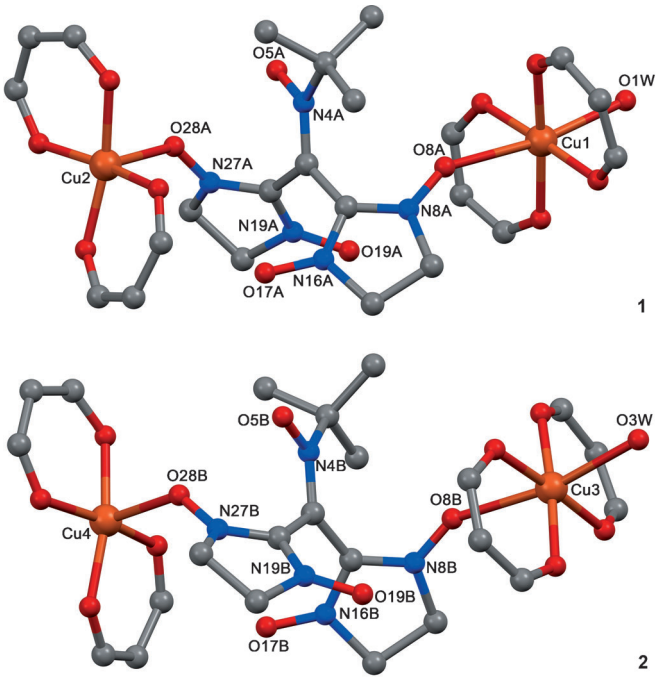

Figure 7. The structure of the two crystallographically independent molecules (**1** and **2**) of [{Cu(hfac)$_2$}$_2$(**DR^1**)(H$_2$O)] (**10**).

show that coordination of the diradical **DR^1** by Cu^{II} leads to very small geometry changes in the ligand (Table 1).

The unit cell of compound **10** consists of two crystallographically independent molecules [{Cu(hfac)$_2$}$_2$(**DR^1**)(H$_2$O)] (Figure 7). In both molecules (**1** and **2**), the paramagnetic ligands **DR^1** are coordinated through O atoms of the nitronyl nitroxide fragments and bridge two {Cu(hfac)$_2$} matrices. The O atom of one nitronyl nitroxide fragment occupies the vertex of the square pyramid of the penta-coordinated Cu atom (Cu(2)–O(28a) 2.237(2) Å, Cu(4)–O(28b) 2.240(2)). The O atom of another nitronyl nitroxide fragment takes one of the axial positions of the hexa-coordinated Cu atom (Cu(1)–O(8a) 2.535(2) Å, Cu(3)–O(8b) 2.460(2)), and the other axial position is occupied by an O atom of a water molecule (Cu(1)–O(1w) 2.336(3) Å, Cu(3)–O(3w) 2.349(3)). The distances Cu–O$_{hfac}$ for Cu(1) and Cu(3) fall in the range 1.919(3)–1.948(3) Å, and for Cu(2) and Cu(4) in the range 1.938(3)–1.963(3) Å, the angles at the coordinated atoms O$_{NO}$ are equal to 131.0(2), 132.2(2), 144.5(2) and 147.2(2)° for O(28b), O(28a), O(8b) and O(8a), respectively. The described geometric parameters of the complexes are practically retained upon cooling to 85 K (Table 3).

In the structure of co-crystallised **11**, the fragments [{Cu(hfac)$_2$}$_2$(**DR^1**)(H$_2$O)] and [Cu(hfac)$_2$(H$_2$O)] are bridged by hydrogen bonds to form chains (Figure 8). In binuclear fragment [{Cu(hfac)$_2$}$_2$(**DR^1**)(H$_2$O)], the O atoms of one of the nitronyl nitroxide fragments of **DR^1** and a water molecule occupy the vertices of the square bipyramid at the Cu(2) atom (Figure 8, distances: Cu–O$_{NO}$ 2.612(4), Cu–O$_{hfac}$ 1.936(4)–1.944(4) Å; angle at O$_{NO}$: 150.8(3)°, distance: Cu–O$_{H_2O}$ 2.282(4) Å). In addition, **DR^1** forms, with Cu(1), a seven-membered chelate ring by coordinating through O atoms of another nitronyl nitroxide frag-

Table 3. Bond lengths [Å] and angles [°] in N–O–Cu fragments of the coordinated diradical **DR**[1] in complexes **10** and **11**.

	10				**11**
T [K]	85		240		295
type of molecule	**1**	**2**	**1**	**2**	
Cu–O(28)	2.231(3)	2.260(3)	2.237(2	2.240(2)	1.962(4)
∡CuO(28)N(27)	131.8(3)	129.2(3)	132.2(2)	131.0(2)	121.8(3)
Cu–O(8)	2.487(3)	2.407(3)	2.535(2)	2.460(2)	2.612(4)
∡CuO(8)N(8)	147.8(3)	142.8(3)	147.2(2)	144.5(2)	150.8(3)
Cu–O(5)					2.391(4)
∡CuO(5)N(4)					127.9(3)

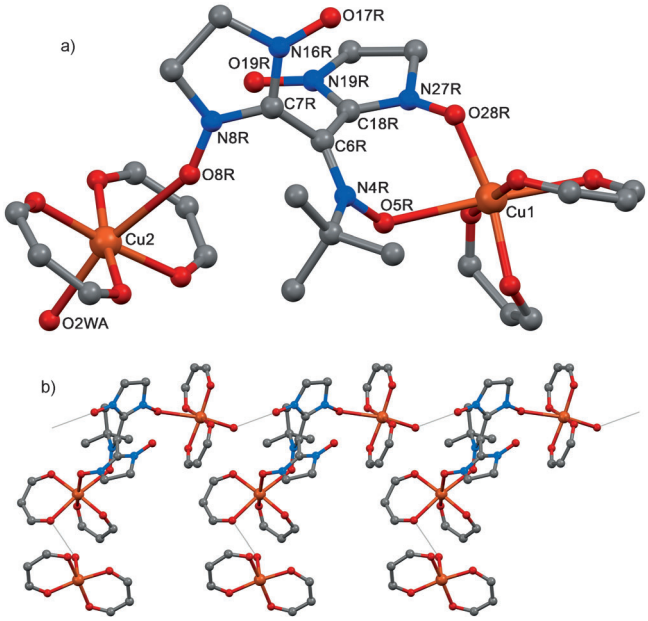

Figure 8. The structure of a) the [{Cu(hfac)$_2$}$_2$(**DR**[1])(H$_2$O)] fragment and b) the chain in the structure of [{Cu(hfac)$_2$}$_2$(**DR**[1])(H$_2$O)][Cu(hfac)$_2$(H$_2$O)] (**11**).

ment and nitrone group (distance Cu–O$_{NO}$: 1.962(4) and 2.391(4) Å, angle at atom O$_{NO}$: 121.8(3) and 127.9(3)°, respectively; distance Cu–O$_{hfac}$: 1.937(4)–1.963(3) Å). The short Cu(1)–O$_{NO}$ distance (1.962(4) Å) implies a strong AF interaction of the unpaired electrons in the Cu^{II} ion and the radical centre at this coordination site.

Figure 9 shows the temperature dependence of the magnetic susceptibility (χ) for complexes **10** and **11**, represented in the form χT. The value of χT for **10** (circles) is equal to 1.84 cm^3 K mol^{-1} at 300 K and increases with decreasing temperature to 2.04 at 30 K, and then abruptly drops to 1.47 at 5 K. It is clear that at 300 K the temperature dependence of χT has not yet reached saturation. Thus, the high temperature value of χT is noticeably higher than the theoretical, purely spin value of 1.5 cm^3 K mol^{-1} obtained by summing the contributions from four non-interacting paramagnetic centres, two Cu^{II} ions ($S=1/2$) and diradical **DR**[1] (two weakly interacting spins $S=1/2$), with $g=2$. The increase in χT indicates dominating FM exchange interactions, whereas the decrease below 30 K comes from weaker AF intramolecular exchange interactions.

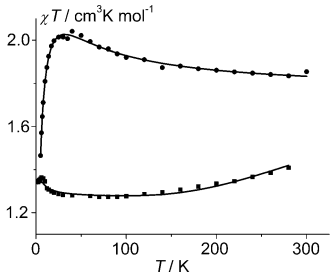

Figure 9. The experimental χT temperature dependence of the polycrystalline samples of **10** (circles) and **11** (squares). Solid curves are the theoretical simulations, performed as described in the text. The *g* values for the radical centres in **DR**[1] were fixed at 2.0. The best fitting for **10** corresponds to $J_{DR^1}/k=-4.1$ K, $g_{Cu}=2.33$, $J_1/k=42.7$ K, $J_2/k=14.1$ K and $\theta=-1.15$ K. The best fitting for **11** corresponds to $J_{DR^1}/k=-11.3$ K, $g_{Cu}=2.25$, $J_1/k=-416.1$ K, $J_2/k=+2.4$ K and $\theta=-0.34$ K.

A qualitatively different temperature dependence of χT was obtained for the polycrystalline sample of compound **11** (Figure 9, squares). The value of χT, equal to 1.41 cm^3 K mol^{-1} at 280 K, gradually decreases with decreasing temperature and reaches a plateau at approximately 1.28 in the range 100–40 K, and then increases again, reaching 1.37 at 6 K. The initial decrease in χT and the fact that the high temperature value is significantly lower than the theoretical, purely spin value of 1.875 cm^3 K mol^{-1} for five non-interacting paramagnetic centres (three Cu^{II} ions with $S=1/2$ and diradical **DR**[1] with two spins $S=1/2$, $g=2.0$) indicate a strong AF exchange interaction in the equatorial fragment Cu(1)–**DR**[1]. The value of χT in the region of the plateau is close to the theoretical, purely spin value of 1.125 cm^3 K mol^{-1} for three non-interacting $S=1/2$ centres at a g value of 2. The increase in χT with a further decrease in temperature below 40 K indicates weak FM exchange interactions.

To enable an understanding at the molecular level and to perform correct simulation of the magnetic properties of the compounds **10** and **11**, the intramolecular pair exchange interactions have been calculated for the XRD structures (Figures 7 and 8). Taking into account the disjoint nature of diradical **DR**[1], we employed a simplified model to calculate the parameters of the exchange interactions between Cu^{II} ions and **DR**[1] (J_1 and J_2). As shown previously (Figure 5), the spin density in **DR**[1] is localised almost exclusively on the nitronyl nitroxide fragments. Therefore, it is reasonable to split the diradical into two radical fragments. Figure S9 in the Supporting Information shows these fragments and the atomic spin-density distribution for **DR**[1] and model radical fragments. This figure demonstrates that the atomic spin-density distributions in the model radicals are almost the same as in the corresponding nitronyl nitroxide moieties of the diradical **DR**[1]. Thus, to estimate parameters J_1 and J_2, we performed calculations for the Cu(hfac)$_2$ complexes with the model radicals. Figure 10 shows selected structures of such complexes for compounds **10** and **11**.

It has previously been demonstrated that the spin-unrestricted broken-symmetry approach at the DFT level is well suited for calculation of the *J* value between the Cu(hfac)$_2$ matrix and nitroxide radicals.[23] Thus, we used the same approach in our

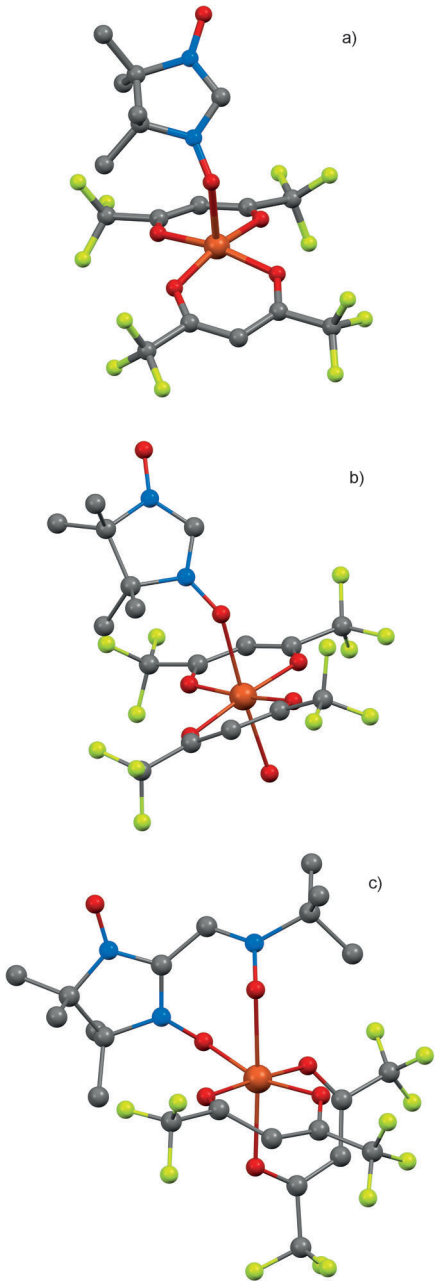

Figure 10. Three types of the Cu(hfac)$_2$ complexes with model radicals employed in the calculation of the exchange interactions for compounds **10** (a and b) and **11** (b and c).

model calculations. For compound **10**, the calculations predict only ferromagnetic exchange interactions between the radical fragments of **DR**^{1} and both Cu(hfac)$_2$ units (Table 4). Furthermore, the *J* values calculated for crystallographically independent molecules **1** and **2** (Figure 7) are similar, and the larger values are the same ($J/k \approx 53$ K, Table 4). In contrast with **10**, the calculations for **11** predict both FM and AF interactions, and the latter interactions are much stronger than the former. Atomic spin-density distributions in the model complexes are presented in the Supporting Information (Figure S10). In addition, we calculated g tensors for the Cu complexes (for details, see the Supporting Information). For all complexes, the g tensors were found to be slightly anisotropic with $g_{iso} \approx 2.11$ (Table S2 in the Supporting Information).

Table 4. Parameters of the pair exchange interactions (J/k [K]) between Cu(hfac)$_2$ units and model radical fragments of the coordinated diradical **DR**^{1} calculated by using the spin-unrestricted broken-symmetry approach at the (U)B3LYP/SVP and (U)B3LYP/TZVP (in parentheses) levels of theory for the XRD geometry (for **10** at 240 K) in complexes **10** and **11**. Experimental *J* values correspond to the best fitting of the temperature dependences of the magnetic susceptibility.

	10			**11**	
	1 (calcd)	**2** (calcd)	exptl	calcd	exptl
*r*Cu–O [Å]	2.237	2.240		1.962	
J/k [K]	53.7 (54.9)	53.1	42.7	–1141.2	–416.1
*r*Cu–O [Å]	2.535	2.460		2.391	
J/k [K]	14.4 (14.5)	29.2	14.1	8.3	2.4
J_{DR^1}/k, [K]	–	–	−4.1		−11.3

The results of calculation of the *J* values (Table 4) are qualitatively clear. In the case of **10**, both nitronyl nitroxide fragments are coordinated in the axial positions to the Cu(hfac)$_2$ complex (Figure 10a, 10b). On the other hand, in compound **11**, only one nitronyl nitroxide fragment is coordinated in the axial position (Figure 10b), and the second fragment is coordinated in the equatorial position (Figure 10c). The strong AF coupling of the Cu(hfac)$_2$ unit with the nitronyl nitoxide radical fragment in the equatorial position is caused by the very short Cu–O bond length (1.962 Å) and hence a large overlap of the SOMOs (the $d_{x^2-y^2}$ orbital of the Cu ion and the π-SOMO of the radical fragment, Figure S11 in the Supporting Information).

The experimental χT dependence for compound **10** was approximated theoretically by using the isotropic spin Hamiltonian [Eq. (3)].

$$\hat{H} = -2\sum_{i=1}^{3}\sum_{j=i+1}^{4} J_{ij}\,\hat{\vec{S}}_i\,\hat{\vec{S}}_j + \sum_{i=1}^{4} g_{ii}\beta\,\hat{\vec{S}}_i\,\hat{\vec{B}} \qquad (3)$$

The calculated parameters of the magnetic coupling of the Cu(hfac)$_2$ units and model radical fragments (Table 4) and the experimental value of $J/k = -7.4$ K for **DR**^{1} were taken as the initial guess in the fitting procedure. The best fitting is in very good agreement with the experiments (Figure 9, upper curve) and corresponds to the following optimised parameters of the spin Hamiltonian in Equation (3): $J_{DR^1}/k = -4.1$, $J_1/k = 42.7$, $J_2/k = 14.1$ K, $g_{Cu} = 2.33$. The intercluster interactions were also taken into account through the Weiss temperature, $\theta_W = -1.15$ K, as a shift of the temperature scale, $kT' = k(T - \theta_W)$. Thus, the **DR**^{1} ligand is strongly ferromagnetically coupled ($J_1/k = 42.7$ K) with only one Cu^{II} ion and the interaction with another Cu^{II} ion is three times weaker ($J_2/k = 14.1$ K). Note that both experimental values are in good agreement with the calculations (Table 4). The AF coupling in the **DR**^{1} fragment of **10** ($J/k = -4.1$ K) is similar to the value measured for the sample of pure **DR**^{1} ($J/k = -7.4$ K), which agrees with the similarity in the geometry of the diradicals in both compounds (Table 1).

According to our DFT calculations (Figure S12 in the Supporting Information), the exchange interactions between the

[{Cu(hfac)$_2$}$_2$(**DR^1**)(H$_2$O)] and [Cu(hfac)$_2$(H$_2$O)] units, as well as the intercluster exchange interactions, in compound **11** are negligible. Thus, prior to simulation, the contribution to χT from the [Cu(hfac)$_2$(H$_2$O)] unit was subtracted, assuming $g=2.11$. The residual part of χT was simulated by using the same spin Hamiltonian [Eq. (3)]. As for compound **10**, the computationally predicted J values (Table 3) were taken to be the initially guessed values. The following parameters $J_{DR^1}/k=-11.3$, $J_1/k=-416.1$, $J_2/k=2.4$ K and $g_{Cu}=2.25$ led to the best agreement of theory and experiment (Figure 9, lower curve). The intercluster interactions were also taken into account through the Weiss temperature $\theta=-0.34$ K. Table 4 demonstrates that the optimal parameters are in reasonable agreement with our calculations.

Conclusion

Herein, the first representatives of the C(sp^2)-spaced nitronyl nitroxide (**DR^1**) and iminonitroxide (**DR^2**) diradicals have been synthesised. Diradical **DR^1** was prepared by using the reaction of the silicon derivative of *N*-*tert*-butylmethanimine oxide with the lithium derivative of the Ullman nitronyl nitroxide. **DR^1** was then reduced in the NaNO$_2$/AcOH system to the corresponding iminonitroxide diradical **DR^2**. **DR^1** and **DR^2** are the heteroatom analogues of 1,1,2,3,3-pentamethylenepropane (PMP), a classic disjoint hydrocarbon diradical with a small singlet–triplet splitting (ΔE_{ST}). According to our DFT and ab initio calculations, the value of ΔE_{ST} for PMP depends on its geometry and is positive for the planar C_{2v} structure and negative for the optimized C_2 structure. **DR^1** and **DR^2**, being heteroatom analogues of PMP, have significantly smaller ΔE_{ST} values, which is typical of the hetero-substitution of hydrocarbon diradicals.

Two heterospin complexes [{Cu(hfac)$_2$}$_2$(**DR^1**)(H$_2$O)] (**10**) and [{Cu(hfac)$_2$}$_2$(**DR^1**)(H$_2$O)][Cu(hfac)$_2$(H$_2$O)] (**11**) were synthesised. Sufficiently strong FM couplings of **DR^1** with both Cu^{II} ions (J_1/k=42.7 and 14.1 K) were detected for compound **10**. In turn, a very strong AF interaction ($J/k=-416$ K) between the Cu^{II} ion and **DR^1** coordinated in the equatorial position to the former was revealed for compound **11**. Thus, the resulting heterospin systems can exhibit essentially different magnetic properties. In any case, transition-metal complexes with newly designed diradicals represent a formidable but exciting challenge.

Experimental Section

Reagents and general methods

4,4,5,5-Tetramethyl-4,5-dihydro-1*H*-imidazol-3-oxide-1-oxyl was synthesised as reported previously;[9b] [Cu(hfac)$_2$][24] was sublimed before use; and THF was freshly distilled over sodium hydride. Other chemicals were of the highest purity commercially available and used as received. The progress of reactions was monitored by TLC on Silica gel 60 F$_{254}$ aluminium sheets. Chromatography was carried out with silica gel (0.063–0.200 mm) for column chromatography. FTIR spectra were taken on KBr pellets on a Bruker Vector-22 spectrometer. Elemental analyses were performed by using a Euro EA 3000 elemental analyzer.

N-{Bis(4,4,5,5-tetramethyl-3-oxido-1-oxyl-4,5-dihydro-1*H*-imidazol-2-yl)methylene}-2-methylpropan-2-amine oxide (DR^1)

A solution of LiN(SiMe$_3$)$_2$ (1.0 M; 32.1 mL, 32.1 mmol) in THF was added at −90 °C under an argon atmosphere to a vigorously stirred solution of 4,4,5,5-tetramethyl-4,5-dihydro-1*H*-imidazol-3-oxide-1-oxyl (4.8 g, 30.5 mmol) in anhydrous THF (50 mL). The reaction mixture was stirred at −90 °C for 30 min. A solution of freshly prepared *N*-*tert*-butyl-*N*-methylene-*O*-(trimethylsilyl)hydroxylammonium chloride (**4**; 3.2 g, 15.3 mmol) in THF (15 mL) was then added at −90 °C under an argon atmosphere. After 1 h, the cooling bath was removed and the reaction mixture was allowed to warm to room temperature; the reaction mixture became a reddish-brown suspension. Concentrated aqueous NH$_4$Cl (10 mL) and CH$_2$Cl$_2$ (100 mL) were successively added. The mixture was stirred for several minutes, then the organic layer was separated off, and the aqueous layer was extracted with CH$_2$Cl$_2$ (1×20 mL). The combined organic layers were washed twice with water, dried over anhydrous Na$_2$SO$_4$, filtered and concentrated under reduced pressure. The residue was dissolved in CH$_2$Cl$_2$ (20 mL), filtered through an Al$_2$O$_3$ layer, ethyl acetate (25 mL) was then added, and CH$_2$Cl$_2$ was evaporated off under reduced pressure. Diradical **DR^1** was collected by filtration and recrystallised from a mixture of heptane with CH$_2$Cl$_2$ (yield: 1.22 g (20%); green crystals). $R_f=0.68$ (ethyl acetate, 0.2 mm alumina N/UV$_{254}$; plastic sheets, Macherey–Nagel); m.p. 164–166 °C; IR: $\tilde{\nu}$ = 432, 471, 543, 699, 752, 874, 1044, 1141, 1176, 1228, 1249, 1284, 1373, 1393, 1416, 1464, 1500, 1620, 2936, 2982, 3010, 3421 cm^{-1}; elemental analysis calcd (%) for C$_{19}$H$_{33}$N$_5$O$_5$: C 55.5, H 8.1, N 17.0; found: C 55.3, H 7.9, N 16.8.

N-{Bis(4,4,5,5-tetramethyl-1-oxyl-4,5-dihydro-1*H*-imidazol-2-yl)methylene}-2-methylpropan-2-amine oxide (DR^2)

A mixture of diradical **DR^1** (500 mg, 1.22 mmol), NaNO$_2$ (336 mg, 4.9 mmol), CHCl$_3$ (25 mL), HOAc (0.2 mL) and H$_2$O (0.2 mL) was stirred at 40–45 °C until the starting nitronyl nitroxide was completely consumed (30 min). The cooled reaction mixture was neutralised with a saturated aqueous solution of NaHCO$_3$, the organic layer was separated off and dried over anhydrous Na$_2$SO$_4$, filtered through a layer of Al$_2$O$_3$ (2×5 cm, EtOAc as eluent) and evaporated under reduced pressure. The residue was recrystallised from a mixture of heptane and CH$_2$Cl$_2$ (yield: 370 mg (80%); red crystals). $R_f=0.71$ (ethyl acetate on Silica gel 60 F$_{254}$; aluminium sheets, Merck); m.p. 136–137 °C; IR: $\tilde{\nu}$ = 462, 514, 532, 555, 592, 640, 682, 702, 779, 803, 832, 872, 963, 1102, 1144, 1155, 1202, 1237, 1313, 1364, 1391, 1453, 1497, 1534, 1569, 1640, 2935, 2979, 2997, 3017, 3444 cm^{-1}; elemental analysis calcd (%) for C$_{19}$H$_{33}$N$_5$O$_3$: C 60.1, H 8.8, N 18.5; found: C 60.0, H 8.3, N 18.5.

Complex 10

A mixture of diradical **DR^1** (20 mg, 0.05 mmol) and [Cu(hfac)$_2$] (46.4 mg, 0.10 mmol) was dissolved in CH$_2$Cl$_2$ (2 mL). The solvent was removed with a gentle flow of air, and the residue was dissolved in hexane (6 mL). The resulting solution was kept at approximately 6 °C overnight. The dark-brown crystals suitable for XRD analysis were filtered off, washed with cold hexane, and dried in air (yield: 37 mg (55%)). Elemental analysis calcd (%) for Cu$_2$C$_{39}$F$_{24}$H$_{39}$N$_5$O$_{14}$: C 33.8, H 2.8, N 5.1, F 32.9; found: C 34.2, H 3.3, N 5.2, F 33.1.

Complex 11

A mixture of diradical **DR[1]** (20 mg, 0.05 mmol) and [Cu(hfac)$_2$] (70.0 mg, 0.15 mmol) was dissolved in CH_2Cl_2 (2 mL). Hexane (4 mL) was then added. The resulting solution was kept at approximately 6 °C overnight. The dark-brown crystals suitable for XRD analysis were filtered off, washed with cold hexane, and dried in air (yield: 65 mg (71 %)). Elemental analysis calcd (%) for $Cu_3C_{49}F_{36}H_{43}N_5O_{19}$: C 31.3, H 2.3, N 3.7, F 36.4; found: C 31.5, H 2.9, N 3.9, F 36.2.

X-ray structure analysis

Intensity data for single crystals of **DR[1]**, **DR[2]**, **10** and **11** were collected at room temperature by using graphite monochromatised $Mo_{K\alpha}$ radiation ($\lambda = 0.71073$ Å). The structures were solved by direct methods and refined by the block-diagonal method for compound **10** and by the full-matrix least-squares method on F^2 for other compounds. The positions of H atoms were calculated geometrically and refined isotropically by using the riding model.

CCDC-925360 (**DR[1]**), CCDC-925361 (**DR[2]**), CCDC-925362 (**10** at 240 K), CCDC-925363 (**10** at 85 K), CCDC-935331 (**6**), CCDC-935332 (**7**), and CCDC-935333 (**11**) contain the supplementary crystallographic data for this paper. These data can be obtained free of charge from The Cambridge Crystallographic Data Centre via www.ccdc.cam.ac.uk/data_request/cif.

Crystallographic data for DR[1]: $C_{19}H_{33}N_5O_5$; $M_r = 411.50$; $T = 296$ K; monoclinic; $P2_1/n$; $a = 10.2991(6)$, $b = 11.7949(6)$, $c = 17.9026(10)$ Å; $\beta = 93.859(4)°$; $V = 2169.8(2)$ Å^3; $Z = 4$; $D_{calcd} = 1.260$ g cm^{-3}; $\mu(Mo_{K\alpha}) = 0.092$ mm^{-1}; a total of 17561 reflections ($\theta_{max} = 28.07°$); 5211 unique reflections ($R_{int} = 0.0700$); 2547 ($F > 4\sigma_F$); 263 parameters; GOOF = 0.847; $R1 = 0.0494$; $wR2 = 0.1107$ ($I > 2\sigma_I$); $R1 = 0.1000$; $wR2 = 0.1256$ (all data); max/min difference peak 0.212/−0.189 e Å^{-3}.

Crystallographic data for DR[2]: $C_{19}H_{33}N_5O_3$; $M_r = 379.50$; $T = 240$ K; monoclinic; $P2_1/n$; $a = 10.593(2)$, $b = 11.391(2)$, $c = 18.011(4)$ Å; $\beta = 94.176(5)°$; $V = 2167.4(7)$ Å^3; $Z = 4$; $D_{calcd} = 1.163$ g cm^{-3}; $\mu(Mo_{K\alpha}) = 0.080$ mm^{-1}; a total of 17630 reflections ($\theta_{max} = 28.37°$); 5391 unique reflections ($R_{int} = 0.0914$); 1920 ($F > 4\sigma_F$); 224 parameters; GOOF = 0.691; $R1 = 0.0507$; $wR2 = 0.1009$ ($I > 2\sigma_I$); $R1 = 0.1487$; $wR2 = 0.1277$ (all data); max/min difference peak 0.187/−0.189 e Å^{-3}.

Crystallographic data for 10 at 240 K: $C_{39}H_{39}Cu_2F_{24}N_5O_{14}$; $M_r = 1384.83$; triclinic; $P\bar{1}$; $a = 11.6488(10)$, $b = 19.8802(17)$, $c = 24.205(2)$ Å; $\alpha = 95.737(2)$, $\beta = 90.965(2)$, $\gamma = 91.021(2)°$; $V = 5575.4(8)$ Å^3; $Z = 4$; $D_{calcd} = 1.650$ g cm^{-3}; $\mu(Mo_{K\alpha}) = 0.906$ mm^{-1}; a total of 92397 reflections ($\theta_{max} = 28.09°$); 26863 unique reflections ($R_{int} = 0.0666$); 13615 ($I > 2\sigma_I$); 1708 parameters; GOOF = 0.949; $R1 = 0.0558$; $wR2 = 0.1536$ ($I > 2\sigma_I$); $R1 = 0.1117$; $wR2 = 0.1719$ (all data); max/min difference peak 0.764/−0.664 e Å^{-3}.

Crystallographic data for 10 at 85 K: $C_{39}H_{39}Cu_2F_{24}N_5O_{14}$; $M_r = 1384.83$; triclinic; $P\bar{1}$; $a = 11.4825(17)$, $b = 19.751(3)$, $c = 23.873(4)$ Å; $\alpha = 95.749(3)$, $\beta = 91.245(3)$, $\gamma = 90.772(3)°$; $V = 5385.1(14)$ Å^3; $Z = 4$; $D_{calcd} = 1.708$ g cm^{-3}; $\mu(Mo_{K\alpha}) = 0.938$ mm^{-1}; a total of 95345 reflections ($\theta_{max} = 27.99°$); 25696 unique reflections ($R_{int} = 0.0808$); 16847 ($I > 2\sigma_I$); 1526 parameters; GOOF = 1.048; $R1 = 0.0611$; $wR2 = 0.1685$ ($I > 2\sigma_I$); $R1 = 0.0932$; $wR2 = 0.1787$ (all data); max/min difference peak 1.653/−1.155 e Å^{-3}.

Crystallographic data for 11: $C_{49}H_{43}Cu_3F_{36}N_5O_{19}$; $M_r = 1880.50$; triclinic; $P\bar{1}$; $a = 11.0607(5)$, $b = 17.1007(9)$, $c = 19.3418(10)$ Å; $\alpha = 88.455(4)$, $\beta = 87.600(3)$, $\gamma = 85.574(3)°$; $V = 3643.3(3)$ Å^3; $Z = 2$; $D_{calcd} = 1.714$ g cm^{-3}; $\mu(Cu_{K\alpha}) = 2.493$ mm^{-1}; a total of 31421 reflections ($\theta_{max} = 60.04°$); 9989 unique reflections ($R_{int} = 0.1178$); 4765 ($I > 2\sigma_I$); 1165 parameters; GOOF = 0.893; $R1 = 0.0558$; $wR2 = 0.1286$ ($I > 2\sigma_I$); $R1 = 0.1214$; $wR2 = 0.1479$ (all data); max/min difference peak 0.355/−0.278 e Å^{-3}.

EPR spectroscopy

EPR spectra of diradical **DR[2]** were taken in *ortho*-terphenyl glass at $T = 200$ K on BRUKER EMX and BRUKER ELEXSYS E580 EPR spectrometers. Crystals of **DR[2]** (about 0.01 % w/w) were mixed with polycrystalline *ortho*-terphenyl in a standard 5 mm quartz EPR tube. The mixture was molten in moderately hot water; the tube was quenched in liquid nitrogen to produce glass and transferred to the pre-cooled spectrometer sample compartment for analysis. EPR spectra of diradical **DR[1]** were taken at tenfold dilution due to its lower solubility in *ortho*-terphenyl.

Magnetic measurements

The magnetic susceptibility of the polycrystalline samples was measured with a Quantum Design MPMSXL SQUID magnetometer in the temperature range 2–300 K with a magnetic field of up to 5 kOe. None of the complexes exhibited any field dependence of molar magnetization at low temperatures. Diamagnetic corrections were made by using the Pascal constants.[25]

Computational details

As the spin-orbit contribution to the ZFS of organic diradicals is expected to be negligible,[26] the spin–spin part of the D tensor was only calculated by using the approach of the Neese group[27] implemented in the ORCA package.[28] The spin-restricted open-shell DFT approach with a pure BP88 functional[14a,b] and TZVP basis set[14] was used for calculations of the ZFS. The J values were calculated by using two different approaches. First, the spin-unrestricted broken-symmetry (BS) approach[29] was employed [Eq. (4)], in which E^{HS} is the energy of the high-spin state and E_{BS}^{LS} is the energy of the low-spin state within the spin-unrestricted broken-symmetry (BS) approach. The energies were calculated at the UB3LYP level of theory[15] with use of ORCA[28] and the GAUSSIAN 09 suite of programs.[30] In all cases, the S^2 values for the high-spin triplet and low-spin broken-symmetry states fall into the intervals 2.04–2.09 and 1.04–1.07, respectively. The only exception is the diradical **DR[2]** with slightly higher S^2 values (2.16 and 1.11, respectively). In addition, the singlet–triplet splitting ($2J$) in diradicals **DR[1]**, **DR[2]** and PMP were calculated by using the multi-reference CASSCF and CASSCF/NEVPT2 procedures,[31] implemented in the ORCA package.[28] The julX program, written by E. Bill, was used for the simulation of the temperature dependence of the magnetic susceptibility.[32]

$$J = -(E^{HS} - E_{BS}^{LS})/(\langle S^2\rangle^{HS} - \langle S^2\rangle_{BS}^{LS}) \quad (4)$$

Acknowledgements

This study was supported by the Ministry of Education and Science of the Russian Federation (projects 8436 and 14.132.21.1451), the Russian Foundation for Basic Research (grants 12–03–00067, 12–03–31184, 11–03–00158, 12–03–33010, and 13–03–12401), the President grants (MD-276.2014.3,MK-6497.2 012.3, MK-1662.2012.3 and MK-5791.2013.3), the Russian Academy of Sciences, the Siberian Branch of RAS and the Siberian Supercomputer Center. E.A.S. appreciates support from the Dynasty Foundation and Mikhail

Prokhorov Foundation. The authors are grateful to Dr. Alex Kruppa for help in modelling the ESR spectra.

Keywords: EPR spectroscopy · heterospin complexes · nitroxides · quantum chemistry · singlet diradicals · X-ray diffraction

[1] a) *Supramolecular Engineering of Synthetic Metallic Materials: Conductors and Magnets* (Eds.: J. Veciana, C. Rovira, D. B. Amabilino), Kluwer Academic, Dordrecht/Boston/London, **1999**; b) R. G. Hicks in *Stable Radicals: Fundamentals and Applied Aspects of Odd-Electron Compounds*, Wiley, Chichester, **2010**.

[2] a) Y. Masuda, M. Kuratsu, S. Suzuki, M. Kozaki, D. Shiomi, K. Sato, T. Takui, Y. Hosokoshi, X.-Z. Lan, Y. Miyazaki, A. Inaba, K. Okada, *J. Am. Chem. Soc.* **2009**, *131*, 4670 – 4673; b) S. Suzuki, N. Itoh, K. Furuichi, M. Kozaki, D. Shiomi, K. Sato, T. Takui, H. Ohi, S. Itoh, K. Okada, *Chem. Lett.* **2011**, *40*, 22 – 24.

[3] a) A. Caneschi, P. Chiesi, L. David, F. Ferraro, D. Gatteschi, R. Sessoli, *Inorg. Chem.* **1993**, *32*, 1445 – 1453; b) T. Mitsumori, K. Inoue, N. Koga, H. Iwamura, *J. Am. Chem. Soc.* **1995**, *117*, 2467 – 2478; c) K. Inoue, F. Iwahori, A. S. Markosyan, H. Iwamura, *Coord. Chem. Rev.* **2000**, *198*, 219 – 229; d) P. Rabu, M. Drillon, H. Iwamura, G. Görlitz, T. Itoh, K. Matsuda, N. Koga, K. Inoue, *Eur. J. Inorg. Chem.* **2000**, 211 – 216; e) S. V. Fokin, G. V. Romanenko, M. Baumgarten, V. I. Ovcharenko, *J. Struct. Chem.* **2003**, *44*, 864 – 869; f) E. V. Gorelik, V. I. Ovcharenko, M. Baumgarten, *Eur. J. Inorg. Chem.* **2008**, 2837 – 2846.

[4] P. M. Lahti in *Molecule-Based Magnetic Materials: Theory, Techniques, and Applications* (Eds.: M. M. Turnbull, T. Sugimoto, L. K. Thompson), ACS, **1996**, Chapter 14, pp. 218 – 235.

[5] a) D. A. Shultz in *Magnetic Properties of Organic Materials* (Ed.: P. M. Lahti), Marcel Dekker, New York, **1999**, Chapter 6, pp. 103 – 125; b) E. Terada, T. Okamoto, M. Kozaki, M. E. Masaki, D. Shiomi, K. Sato, T. Takui, K. Okada, *J. Org. Chem.* **2005**, *70*, 10073 – 10083.

[6] K. Matsumoto, M. Oda, M. Kozaki, K. Sato, T. Takui, K. Okada, *Tetrahedron Lett.* **1998**, *39*, 6307 – 6310.

[7] *Cambridge Structural Database*, *Version 5.34*, Cambridge Crystallographic Data Center, Cambridge, November 2012 (last update February 2013).

[8] O. N. Chupakhin, I. A. Utepova, M. V. Varaksin, E. V. Tretyakov, G. V. Romanenko, D. V. Stass, V. I. Ovcharenko, *J. Org. Chem.* **2009**, *74*, 2870 – 2872.

[9] a) M. V. Varaksin, E. V. Tretyakov, I. A. Utepova, G. V. Romanenko, A. S. Bogomyakov, D. V. Stass, R. Z. Sagdeev, V. I. Ovcharenko, O. N. Chupakhin, *Russ. Chem. Bull.* **2012**, *61*, 1469 – 1473; b) E. V. Tretyakov, I. A. Utepova, M. V. Varaksin, S. E. Tolstikov, G. V. Romanenko, A. S. Bogomyakov, D. V. Stass, V. I. Ovcharenko, O. N. Chupakhin, *ARKIVOC (Gainesville, FL, U.S.)* **2011**, 76 – 98; c) E. V. Tretyakov, S. E. Tolstikov, G. V. Romanenko, A. S. Bogomyakov, V. K. Cherkasov, D. V. Stass, V. I. Ovcharenko, *Russ. Chem. Bull.* **2011**, *60*, 2325 – 2330.

[10] S. Suzuki, T. Furui, M. Kuratsu, M. Kozaki, D. Shiomi, K. Sato, T. Takui, K. J. Okada, *J. Am. Chem. Soc.* **2010**, *132*, 15908 – 15910.

[11] O. Lagrille, N. R. Cameron, P. A. Lovell, R. Blanchard, A. E. Goeta, R. Koch, *J. Polym. Sci. Part A* **2006**, *44*, 1926 – 1940.

[12] V. N. Parmon, A. I. Kokorin, G. M. Zhidomirov in *Stable Diradicals*, Nauka, Moscow, **1980** (in Russian). (The Library of Congress, link: http://lccn.loc.gov/81478837).

[13] J. A. Weil, J. R. Bolton, J. E. Wertz, *Electron Paramagnetic Resonance: Elementary Theory and Practical Applications*, Wiley, NY, **1994**, p. 164.

[14] a) A. D. Becke, *Phys. Rev. A* **1988**, *38*, 3098 – 3100; b) J. P. Perdew, *Phys. Rev. B* **1986**, *33*, 8822 – 8824; c) F. Weigend, R. Ahlrichs, *Phys. Chem. Chem. Phys.* **2005**, *7*, 3297 – 3305.

[15] a) A. D. Becke, *J. Chem. Phys.* **1993**, *98*, 5648 – 5652; b) C. Lee, W. Yang, R. G. Parr, *Phys. Rev. B* **1988**, *37*, 785 – 789.

[16] A. Schaefer, H. Horn, R. Ahlrichs, *J. Chem. Phys.* **1992**, *97*, 2571 – 2577.

[17] B. Bleaney, K. D. Bowers, *Proc. R. Soc. London Ser. A* **1952**, *214*, 451 – 465.

[18] E. V. Tretyakov, S. E. Tolstikov, G. V. Romanenko, A. S. Bogomyakov, D. V. Stass, A. G. Maryasov, N. P. Gritsan, V. I. Ovcharenko, *Russ. Chem. Bull.* **2011**, *60*, 2608 – 2612.

[19] W. C. Lineberger, W. T. Borden, *Phys. Chem. Chem. Phys.* **2011**, *13*, 11792 – 11813.

[20] W. T. Borden, E. R. Davidson, *J. Am. Chem. Soc.* **1977**, *99*, 4587 – 4594.

[21] M. L. Kearley, A. S. Ichimura, P. M. Lahti, *J. Am. Chem. Soc.* **1995**, *117*, 5235 – 5244.

[22] D. A. Shultz, R. M. Fico Jr., H. Lee, J. W. Kampf, K. Kirschbaum, A. A. Pinkerton, P. D. Boyle, *J. Am. Chem. Soc.* **2003**, *125*, 15426 – 15432.

[23] a) V. I. Ovcharenko, G. V. Romanenko, K. Y. Maryunina, A. S. Bogomyakov, E. V. Gorelik, *Inorg. Chem.* **2008**, *47*, 9537 – 9552; b) E. V. Tretyakov, S. E. Tolstikov, E. V. Gorelik, M. V. Fedin, G. V. Romanenko, A. S. Bogomyakov, V. I. Ovcharenko, *Polyhedron* **2008**, *27*, 739 – 749.

[24] J. A. Bertrand, R. I. Kaplan, *Inorg. Chem.* **1966**, *5*, 489 – 491.

[25] V. T. Kalinnikov, Yu. V. Rakitin in *Introduction in Magnetochemistry. Method of Static Magnetic Susceptibility*, Nauka, Moscow, **1980**, p. 302 (in Russian).

[26] S. Sinnecker, F. Neese, *J. Phys. Chem. A* **2006**, *110*, 12267 – 12275.

[27] a) F. Neese, *J. Am. Chem. Soc.* **2006**, *128*, 10213 – 10222; b) D. Ganyushin, F. Neese, *J. Chem. Phys.* **2006**, *125*, 024103 – 024112.

[28] a) F. Neese, *WIREs Comput. Mol. Sci.* **2012**, *2*, 73 – 78; b) F. Neese, *ORCA-An Ab Initio, Density Functional and Semiempirical Program Package*, *Version 2.9*; Max Planck Institute for Bioinorganic Chemistry, Mulheim, Germany, **2012**.

[29] a) H. Nagao, M. Nishino, Y. Shigeta, T. Soda, Y. Kitagawa, T. Onishi, Y. Yoshika, K. Yamaguchi, *Coord. Chem. Rev.* **2000**, *198*, 265 – 295; b) L. Noodleman, D. A. Case, J. M. Mouesca, *Coord. Chem. Rev.* **1995**, *144*, 199 – 244; c) L. Noodleman, *J. Chem. Phys.* **1981**, *74*, 5737 – 5743.

[30] M. J. Frisch, G. W. Trucks, H. B. Schlegel, G. E. Scuseria, M. A. Robb, J. R. Cheeseman, G. Scalmani, V. Barone, B. Mennucci, G. A. Petersson, H. Nakatsuji, M. Caricato, X. Li, H. P. Hratchian, A. F. Izmaylov, J. Bloino, G. Zheng, J. L. Sonnenberg, M. Hada, M. Ehara, K. Toyota, R. Fukuda, J. Hasegawa, M. Ishida, T. Nakajima, Y. Honda, O. Kitao, H. Nakai, T. Vreven, J. A. Montgomery, Jr., J. E. Peralta, F. Ogliaro, M. Bearpark, J. J. Heyd, E. Brothers, K. N. Kudin, V. N. Staroverov, R. Kobayashi, J. Normand, K. Raghavachari, A. Rendell, J. C. Burant, S. S. Iyengar, J. Tomasi, M. Cossi, N. Rega, J. M. Millam, M. Klene, J. E. Knox, J. B. Cross, V. Bakken, C. Adamo, J. Jaramillo, R. Gomperts, R. E. Stratmann, O. Yazyev, A. J. Austin, R. Cammi, C. Pomelli, J. W. Ochterski, R. L. Martin, K. Morokuma, V. G. Zakrzewski, G. A. Voth, P. Salvador, J. J. Dannenberg, S. Dapprich, A. D. Daniels, Ö. Farkas, J. B. Foresman, J. V. Ortiz, J. Cioslowski, D. J. Fox *Gaussian 09*, *Rev. A.1*, Gaussian, Inc., Wallingford CT, **2009**.

[31] a) C. Angeli, R. Cimiraglia, S. Evangelisti, T. Leininger, J.-P. Malrieu, *J. Chem. Phys.* **2001**, *114*, 10252 – 10264; b) C. Angeli, R. Cimiraglia, J.-P. Malrieu, *J. Chem. Phys.* **2002**, *117*, 9138 – 9153.

[32] Link: http://ewww.mpi-muelheim.mpg.de/bac/logins/bill/julX_en.php.

Received: July 10, 2013
Revised: December 3, 2013

